
INVESTIGATION OF MULTIMODAL AND AGENTIAL INTERACTIONS IN HUMAN-ROBOT IMITATION, BASED ON FRAMEWORKS OF PREDICTIVE CODING AND ACTIVE INFERENCE*

Wataru Ohata

Cognitive Neurorobotics Research Unit
Okinawa Institute of Science and Technology
Okinawa, Japan
wataru.ohata@oist.jp

Jun Tani[†]

Cognitive Neurorobotics Research Unit
Okinawa Institute of Science and Technology
Okinawa, Japan
jun.tani@oist.jp

March 4, 2022

ABSTRACT

This study proposes a model for multimodal, imitative interaction of agents, based on frameworks of predictive coding and active inference, using a variational Bayes recurrent neural network. The model dynamically predicts visual sensation and proprioception simultaneously through generative processes by associating both modalities. It also updates the internal state and generates actions by maximizing the lower bound. A key feature of the model is that the complexity of each modality, as well as of the entire network can be regulated independently. We hypothesize that regulation of complexity offers a common perspective over two distinct properties of embodied agents: coordination of multimodalities and strength of agent intention or belief in social interactions. We evaluate the hypotheses by conducting experiments on imitative human-robot interactions in two different scenarios using the model. First, regulation of complexity was changed between the vision module and the proprioception module during learning. The results showed that complexity of the vision module should be more strongly regulated than that of proprioception because of its greater randomness. Second, the strength of complexity regulation of the whole network in the robot was varied during test imitation after learning. We found that this affects human-robot interactions significantly. With weaker regulation of complexity, the robot tends to move more egocentrically, without adapting to the human counterpart. On the other hand, with stronger regulation, the robot tends to follow its human counterpart by adapting its internal state. Our study concludes that the strength with which complexity is regulated significantly affects the nature of dynamic interactions between different modalities and between individual agents in a social setting.

Keywords predictive coding, active inference, multimodal perception, human-robot interaction, recurrent neural network, variational Bayes, generative model, inference model

1 Introduction

Predictive coding (Rao and Ballard, 1999; Tani and Nolfi, 1999; Lee and Mumford, 2003; Friston, 2005; Hohwy, 2013; Clark, 2015; Friston, 2018) and active inference (Friston et al., 2009, 2010; Baltieri and Buckley, 2017; Buckley et al., 2017; Pezzulo et al., 2018; Oliver et al., 2019) have attracted increasing attention from a variety of research disciplines, such as neuroscience, cognitive science, and psychology, for their potential to provide a unified theoretical framework explaining perception and action generation. They attempt to describe how organisms perceive sensory information and generate actions to act on the environment, so as to minimize surprise.

*This is a preprint.

[†]Corresponding author

Typically, in the formulation of predictive coding, perceptions are modeled using generative models in which the logarithm of marginal likelihood is bounded by the evidence lower bound as:

$$\ln p_{\theta}(\mathbf{X}) \geq \underbrace{\int q_{\phi}(\mathbf{z}|\mathbf{X}) \ln \frac{p_{\theta}(\mathbf{X}, \mathbf{z})}{q_{\phi}(\mathbf{z}|\mathbf{X})} d\mathbf{z}}_{\text{Evidence lower bound}} \quad (1)$$

$$= \underbrace{\mathbb{E}_{q_{\phi}(\mathbf{z}|\mathbf{X})}[\ln p_{\theta}(\mathbf{X}|\mathbf{z})]}_{\text{Accuracy}} - \underbrace{D_{\text{KL}}[q_{\phi}(\mathbf{z}|\mathbf{X})||p(\mathbf{z})]}_{\text{Complexity}} \quad (2)$$

where \mathbf{X} is the observation, \mathbf{z} is the latent variable, $q_{\phi}(\mathbf{z}|\mathbf{X})$ is the approximated posterior, and θ and ϕ are the parameters of the model. The first term of the right side of equation (2) is denominated *accuracy*, which is the expectation of the model with respect to the approximated posterior. The second term on the right side is termed *complexity*, which is the Kullback-Leibler divergence (KL divergence) between the approximated posterior and the prior. The accuracy term represents the reconstruction of the observation with the posterior, and the complexity term serves to regularize the model. The model is optimized by maximizing the lower bound, which is equivalent to minimizing *free energy* proposed by (Friston, 2005).

Recently, Ahmadi and Tani (2019) proposed a network model, the so-called Predictive coding-inspired Variational Recurrent Neural Network (PV-RNN), in which the evidence lower bound is maximized in the processes of perception, action generation, and learning. They introduced a hyper parameter w called the meta-prior, which weights the regulation of the complexity term in the evidence lower bound. They found that a model trained under weaker regulation of the complexity term by setting the meta-prior to a larger value, develops more deterministic dynamics with higher estimated precision, whereas one with stronger regulation by setting the meta-prior to a smaller value does so with more probabilistic dynamics with lower estimated precision. It was found that adequate regulation of complexity by adjusting the meta-prior, contributes greatly to a model’s ability to generalize in learning.

The current study hypothesizes that regulating the complexity term with different strengths should affect cognitive functions of agents in at least two distinct ways, especially for those interacting with others in social settings using multimodal sensation. First, regulating the complexity term with an adequate weighting may enhance effectiveness in coordinating multimodal perceptions. In general our experience is not comprised of a single modality, but of many, such as vision, audio perception, and tactile sensation, and so forth. How those multimodal perceptions can be adequately coordinated for association is not a trivial problem because intrinsic complexity and randomness in spatio-temporal pattern differ in each modality. In this situation, we speculate that such differences between different modalities can be arbitrated by regulating the complexity term of each with an appropriate strength.

Second, regulating the complexity term differently after learning may affect the strength of agent intention or belief in the social interaction. Here, acting with strong intention in social interactions means that an agent acts egocentrically toward others or with volatility, whereas acting with a weak intention means to act passively by following intentions of others. In this regard, Chame and Tani (2019) showed that when the PV-RNN is trained under weaker regulation of the complexity term, the network tends to behave egocentric with less adaptation to sensory inputs, whereas under stronger regulation of the complexity term, the network tends to behave more passively with adaptation to sensor inputs. However, such characteristics of the network, once developed through learning under particular conditions for regulating the complexity term, cannot be changed after learning. In social interactions, agents are better able to act differently, depending on the social context at a given moment. Sometimes they tend to preserve their prior intention for acting perversely, and at other times they change it more easily by adapting to intentions of others. The current study examines such possibilities for modulating behavioral characteristics by dynamically changing parameters to regulate the complexity term during social interaction after learning.

For purposes of evaluating these two hypotheses, we conducted a set of robotics experiments by extending the PV-RNN to facilitate a model of multimodal, agential interaction using visuo-proprioceptive sensory inputs. The model network employed in the current study is comprised of a multi-layered PV-RNN with a branching structure, in which each branch is responsible for one modality. These are connected through an associative module. The model is a generative model and predicts incoming visual perception and proprioception simultaneously through a generative process. This corresponds to the prior generation. The resultant prediction error for each sensory modality is back-propagated through time (Rumelhart et al., 1985) and through each module to the associative module by which the internal state in each module is modulated in the direction of maximization of the evidence lower bound. This corresponds to the posterior inference. The network is trained through supervised learning by maximizing the evidence lower bound. One thing to note is that the model can have different values of the meta-prior in each layer of the PV-RNN in each modality. This means that the model is capable of regulating complexity with different weighting in a layer- and modality-specific manner.

First, we investigated how assigning different values of the meta-prior to the proprioception and vision modules affects learning and the resultant imitation performance with multimodal sensation of visuo-proprioceptive patterns. Our results suggest that regulating complexity more in the vision module than in the proprioception module facilitates better imitation performance in multi-modal sensation after the learning, when visual sensory information contains more randomness than proprioceptive information.

Second, we examined how shifting a set of meta-prior values in the whole network to larger or smaller values than those used in the learning phase affects the characteristics of imitative behavior. We found that the network that strongly regulated the complexity term by setting smaller values of the meta-prior tended to follow human movement patterns by adapting its internal states. On the other hand, the network that weakly regulated the complexity term by setting larger values of the meta-prior tended to generate more egocentric/self-centered movement patterns with less sensitivity to changes or fluctuations in the human movement patterns by adapting its internal state less. The current paper presents a detailed analysis of the underlying mechanisms accounting for these observed phenomena.

The next section describes the employed model in greater detail.

2 Model

2.1 Model overview

This subsection describes briefly how we can model multimodal imitative interaction of agents perceiving visuo-proprioceptive sensory inputs by using concepts of predictive coding and active inference. Among various types of imitation, synchronized imitation is considered in the current study by virtue of its simplicity. In synchronized imitation, the agent is required to imitate target patterns demonstrated by the human counterpart by predicting them on the basis of prior learning. Although target patterns to imitate are structurally the same as previously learned patterns, they could involve marginal variations, as in speed, amplitude, and shape. The process of synchronized imitation can be achieved by means of iterative cycling of prediction of sensory inputs during the demonstration, generation of corresponding movement, and updating the latent state of the network using the resultant sensory prediction error. To generate movement, one step, look-ahead prediction of proprioception is fed to an inverse model (Kawato et al., 1987), which is often implemented by a PID feedback controller in robots. The inverse model or PID feedback controller computes an optimal motor torque as the motor command for minimizing the error between the predicted proprioception (the target joint angles) and the actual proprioception (the actual joint angles). This process of generating adequate motor commands for achieving the expected sensory inputs in terms of the proprioception can be considered a primitive type of active inference (Friston et al., 2010, 2011). Updating the latent state can be performed using a scheme called error regression (Tani and Nolfi, 1999; Ito and Tani, 2004; Hwang et al., 2018; Ahmadi and Tani, 2019), by which the process of sensory perception assumed in a predictive coding framework can be performed.

Now we look at how the PV-RNN (Ahmadi and Tani, 2019) can be used to implement the model for multimodal imitative interaction of robot agents receiving visuo-proprioceptive sensory inputs based on the aforementioned frameworks of predictive coding and active inference. Figure 1 shows the overall system view, consisting of a PV-RNN, a robot, and a human counterpart. The human demonstrates movement patterns to the robot both visually and kinesthetically, guiding the robot’s posture by wearing a motion capture suit.

PV-RNN is considered a generative model, formulated in a continuous spatio-temporal domain, using a variational Bayes framework. A PV-RNN inherits the concept of a Multiple Timescale Recurrent Neural Network (MTRNN) (Yamashita and Tani, 2008), which is characterized by its architecture, which allocates different timescale dynamics to different layers. Higher layers are endowed with slower timescale dynamics and lower layers with faster dynamics, as inspired by recent cognitive neuroscience evidence (Newell et al., 2001; Huys et al., 2004; Smith et al., 2006; Kording et al., 2007). It has been shown that introduction of multiple timescale dynamics can enhance abstraction and generalization in learning by extracting action-primitive hierarchies or chunking structures from observed multimodal sensory inputs (Yamashita and Tani, 2008; Choi and Tani, 2018; Hwang et al., 2018). PV-RNN approximates the posterior at each time step to minimize the reconstruction error in previous steps through variational inference, which is implemented by means of the error regression scheme. Each sensory module for proprioception and vision was modeled with a multi-layered PV-RNN and modules were connected with an associative module, which also consists of a PV-RNN (Figure 1). The associative module generates the top-down prior, conditioned by the current latent state in this module at each time step. The top-down prior is then fed to both the proprioception and vision modules. Each sensory module also generates the top-down prior at each time step conditioned by the previous latent state of the module computed using top-down information provided by the associative module, by which the prediction of sensory inputs, proprioception and vision at the subsequent time step is generated. Here, we note that the actual pixel visual image is compressed into a low-dimensional vector value using a CNN-type (LeCun et al., 1989, 1998) encoder-decoder, which is connected to the bottom layer of the vision PV-RNN module for the purpose of reducing the computational cost. By feeding

the prediction of the next proprioception to the motor controller as the target, the corresponding motor commands for generating expected movements can be generated. When the sensory outcome is observed at each sensory module after the movement, the prediction error is computed. Errors generated in both the proprioceptive and visual modules are back-propagated through time (Werbos, 1974; Rumelhart et al., 1985), as well as through the layers from those sensory modules to the associative module, where the latent state at each layer in each module is updated so as to maximize the lower bound in terms of the posterior inference using the error regression scheme (more details in Section 2.7). This cycle of prediction with the conditional prior, generating the corresponding movement, and updating the latent state in terms of the posterior inference using the error, is repeated at each small Δt of the sensory sampling, where robot agents predict future movement patterns of the human counterpart while updating their own intentions or briefs represented by the latent state for possible adaptation to spontaneous changes or fluctuations.

Finally, learning of demonstrated movement patterns can be done by performing mostly the same cycling process, but by updating connectivity weights without generating actual movement. In this process, the prediction error for the target visuo-proprioceptive sequence patterns sampled in the training exemplar is computed offline without generating movement. The obtained error is used to update the connectivity weights, as well as the latent states, at each time step in the whole network for maximizing the lower bound. Learning is performed in an end-to-end manner across all layers and modules throughout the whole network because the whole network is differentiable.

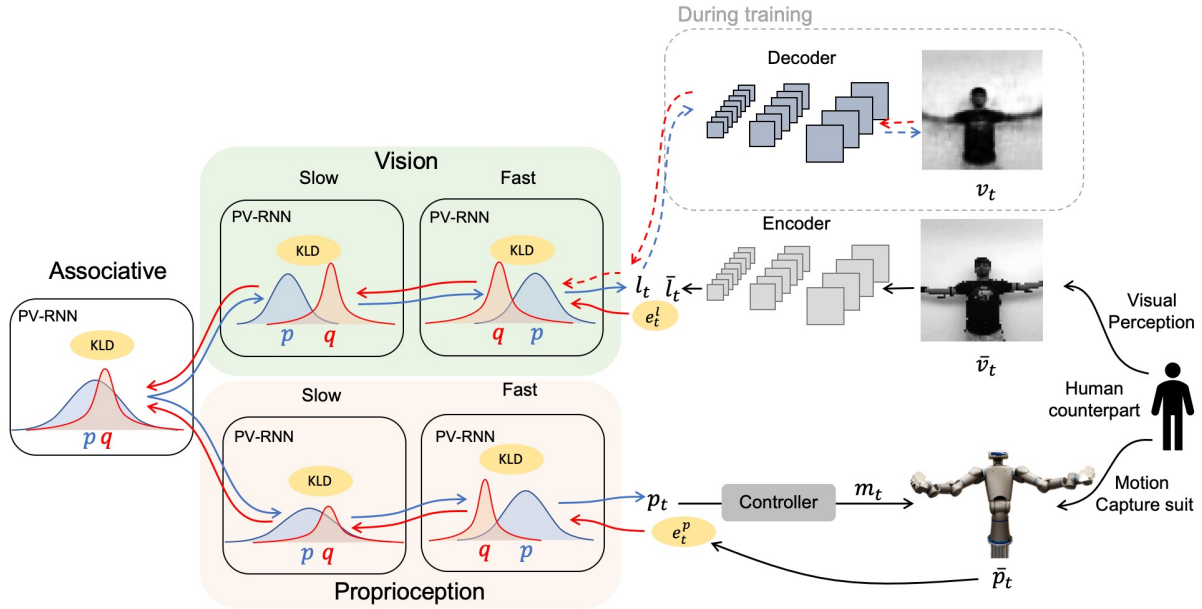


Figure 1: The overall system configuration consists of the PV-RNN, the robot, and the human counterpart, who wears a motion capture suit. The PV-RNN consists of three modules: the associative module, a vision module, and a proprioception module. Each module is comprised of layer(s) of PV-RNN. p and q represent prior and posterior in each layer, and blue arrows illustrate how the top-down intention or brief in terms of the prior, propagates downward through the whole network to predict both sensory modalities. Red arrows illustrate how the bottom-up prediction error in proprioception and vision propagates upward through the whole network to infer the posterior. The PV-RNN layers in the vision module predict the latent dynamics of visual patterns l_t , which are fed to the decoder to generate visual patterns v_t during learning. In error-regression, perceived visual patterns are embedded with the encoder to latent patterns with which the prediction error of visual patterns e_t^l is computed. The proprioception module directly predicts the joint-angle configuration of the robot p_t , which is fed to the motor control system to generate the motor command m_t . The prediction error in proprioception e_t^p is obtained by measuring the actual joint-angle \bar{p}_t . The model is optimized by minimizing the prediction error and KL divergence between the approximated posterior and prior, which is weighted with the meta-prior.

2.2 Derivation of evidence lower bound

PV-RNN is a generative and inference model based on graphical representation (Figure 2). It is comprised of deterministic variables \mathbf{d} , i.e. following Dirac delta distributions, and stochastic variables \mathbf{z} . The model includes prior and infers posterior by variational inference. We modified the original PV-RNN at three points with respect to dependencies of variables. First, in our model, there are no connections between the output of the network \mathbf{x} and \mathbf{z} , which exist in the original PV-RNN. This is for simplification of the model, and it was confirmed that removing these connections did not hinder network performance. Second, the current network does not have connections from the lower layer to the higher layer, which the original network does have. This modification is intended to separate more clearly the information flow between top-down generative prediction and bottom-up error propagation. Last, diagonal connections from the higher layer during the previous time-step to the lower layer during the succeeding time-step are changed to vertical connections during the same time-step. Following the derivation of the evidence lower bound in Ahmadi and Tani (2019), the evidence lower bound of the proposed visuo-proprioceptive model is derived as

$$\begin{aligned} \ln(\mathbf{p}_{1:T}, \mathbf{v}_{1:T} | \mathbf{d}_0^*) &\geq \sum_{t=1}^T \left(\mathbb{E}_{q^a, q^p} [\ln P(\mathbf{p}_t | \mathbf{d}_t^{p,1})] + \mathbb{E}_{q^a, q^v} [\ln P(\mathbf{v}_t | \mathbf{d}_t^{v,1})] \right. \\ &\quad - \sum_{l \in A} D_{\text{KL}}[q(\mathbf{z}_t^l | \mathbf{d}_{t-1}^l, e_{t:T}^p, e_{t:T}^v) \| p(\mathbf{z}_t^l | \mathbf{d}_{t-1}^l)] \\ &\quad - \sum_{l \in P} D_{\text{KL}}[q(\mathbf{z}_t^l | \mathbf{d}_{t-1}^l, e_{t:T}^p) \| p(\mathbf{z}_t^l | \mathbf{d}_{t-1}^l)] \\ &\quad \left. - \sum_{l \in V} D_{\text{KL}}[q(\mathbf{z}_t^l | \mathbf{d}_{t-1}^l, e_{t:T}^v) \| p(\mathbf{z}_t^l | \mathbf{d}_{t-1}^l)] \right) \end{aligned} \quad (3)$$

where A, P, and V represent the associative module, the proprioception module, and the vision module, respectively, and l indicates a layer in each module. $\mathbf{p}_{1:T}$ and $\mathbf{v}_{1:T}$ are time series proprioceptive and visual patterns. \mathbf{d}_0^* represents \mathbf{d} in all the layers at time-step 0. \mathbb{E}_{q^a, q^p} denotes the expectation over all the distributions of \mathbf{z} in the associative module and the proprioception module, and \mathbb{E}_{q^a, q^v} denotes expectation over all distributions of \mathbf{z} in the associative module and the vision module. $\mathbf{d}_t^{p,1}$ is the deterministic valuable in the lowest layer of the proprioception module at time-step t , and $\mathbf{d}_t^{v,q}$ is that in the lowest layer of the vision module. \mathbf{z}_t^l , \mathbf{z}_t^p , \mathbf{z}_t^v are the stochastic variables in l th layer in the associative module, in the proprioception module, and in the vision module at time-step t , respectively. \mathbf{d}_{t-1}^l represents the activities of deterministic variables in l th layer in the associative module, in the proprioception module, and in the vision module at time-step t , respectively. $e_{t:T}^p$ and $e_{t:T}^v$ are the prediction error between the predicted patterns and the target patterns at time-step from t to T in proprioception and vision, respectively. By introducing the meta-prior, which weighs the KL divergence between the approximated posterior and the prior, the evidence lower bound of the model is defined as

$$\begin{aligned} \mathcal{L}_w &:= \sum_{t=1}^T \left(\underbrace{\mathbb{E}_{q^a, q^p} [\ln P(\mathbf{p}_t | \mathbf{d}_t^{p,1})] + \mathbb{E}_{q^a, q^v} [\ln P(\mathbf{v}_t | \mathbf{d}_t^{v,1})]}_{\text{accuracy}} \right. \\ &\quad - \sum_{l \in A} w^l \underbrace{D_{\text{KL}}[q(\mathbf{z}_t^l | \mathbf{d}_{t-1}^l, e_{t:T}^p, e_{t:T}^v) \| p(\mathbf{z}_t^l | \mathbf{d}_{t-1}^l)]}_{\text{complexity in associative module}} \\ &\quad - \sum_{l \in P} w^l \underbrace{D_{\text{KL}}[q(\mathbf{z}_t^l | \mathbf{d}_{t-1}^l, e_{t:T}^p) \| p(\mathbf{z}_t^l | \mathbf{d}_{t-1}^l)]}_{\text{complexity in proprioception module}} \\ &\quad \left. - \sum_{l \in V} w^l \underbrace{D_{\text{KL}}[q(\mathbf{z}_t^l | \mathbf{d}_{t-1}^l, e_{t:T}^v) \| p(\mathbf{z}_t^l | \mathbf{d}_{t-1}^l)]}_{\text{complexity in vision module}} \right) \end{aligned} \quad (4)$$

where w^l represents the meta-priors in the l th layer in the associative module, the proprioception module, and the vision module, respectively. The parameters of the model are optimized by maximizing the lower bound, which corresponds to minimizing the free energy.

2.3 The associative module

The associative module is comprised of a PV-RNN. Since we adopted MTRNN in PV-RNN, its computations are as follows.

$$\mathbf{u}_t^{a,l} = \begin{cases} \mathbf{W}_{dd}^{a,ll} \mathbf{d}_{t-1}^{a,l} + \mathbf{W}_{dz}^{a,ll} \mathbf{z}_t^{a,l} + \mathbf{b}^{a,l} & \text{if top layer} \\ \mathbf{W}_{dd}^{a,ll} \mathbf{d}_{t-1}^{a,l} + \mathbf{W}_{dd}^{a,ll+1} \mathbf{d}_t^{a,l+1} + \mathbf{W}_{dz}^{a,l} \mathbf{z}_t^{a,l} + \mathbf{b}^{a,l} & \text{otherwise} \end{cases} \quad (5)$$

$$\mathbf{h}_t^{a,l} = \left(1 - \frac{1}{\tau^{a,l}}\right) \mathbf{h}_{t-1}^{a,l} + \frac{1}{\tau^{a,l}} \mathbf{u}_t^{a,l} \quad (7)$$

$$\mathbf{d}_t^{a,l} = \tanh(\mathbf{h}_t^{a,l}) \quad (8)$$

where $\mathbf{u}_t^{a,l}$ is the sum of inputs to l th layer of the associative module. $\mathbf{W}_{dd}^{a,ll}$, $\mathbf{W}_{dz}^{a,ll}$, and $\mathbf{W}_{dd}^{a,ll+1}$ are weight matrices for recurrent connections, the stochastic variable \mathbf{z} , and the input from the higher layer, respectively. $\mathbf{b}^{a,l}$ is the bias in the l th layer in the associative module, and $\tau^{a,l}$ is the time constant for MTRNN computation in the l th layer in the associative module. \tanh is the activation function. The stochastic variable \mathbf{z} is assumed to follow a multivariate Gaussian distribution with diagonal covariant matrix, and the deterministic variable \mathbf{d} predicts mean $\boldsymbol{\mu}$ and variance $\boldsymbol{\sigma}$ of the distribution. That is, for computation of prior,

$$p(\mathbf{z}_t^{p,a,l} | \mathbf{d}_{t-1}^{a,l}) = \mathcal{N}(\mathbf{z}_t^{p,a,l}; \boldsymbol{\mu}_t^{p,a,l}, \boldsymbol{\sigma}_t^{p,a,l}) \quad (9)$$

$$\boldsymbol{\mu}_t^{p,a,l} = \tanh(\mathbf{W}_{\mu d}^{a,l} \mathbf{d}_{t-1}^{a,l} + \mathbf{b}_{\mu}^{a,l}) \quad (10)$$

$$\boldsymbol{\sigma}_t^{p,a,l} = \exp(\mathbf{W}_{\sigma d}^{a,l} \mathbf{d}_{t-1}^{a,l} + \mathbf{b}_{\sigma}^{a,l}) \quad (11)$$

$$\mathbf{z}_t^{p,a,l} = \boldsymbol{\mu}_t^{p,a,l} + \boldsymbol{\sigma}_t^{p,a,l} * \boldsymbol{\epsilon} \quad (12)$$

where $\boldsymbol{\mu}_t^{p,a,l}$ and $\boldsymbol{\sigma}_t^{p,a,l}$ are the mean and variance for the prior distribution of $\mathbf{z}_t^{p,a,l}$ at time-step t in l th layer in the associative module. $\mathbf{W}_{\mu d}^{a,l}$ and $\mathbf{W}_{\sigma d}^{a,l}$ are the weight matrices for $\mathbf{d}_{t-1}^{a,l}$. $\mathbf{b}_{\mu}^{a,l}$ and $\mathbf{b}_{\sigma}^{a,l}$ are the biases for each computation. \tanh in computation of mean is used for stability of optimization, and \exp in $\boldsymbol{\sigma}$ is for variance to be positive. $\boldsymbol{\epsilon}$ is sampled from $\mathcal{N}(\mathbf{0}, \mathbf{I})$. To approximate the posterior, PV-RNN has adaptive variables \mathbf{a} which are specific to time-step and sequence. \mathbf{a} is optimized during learning with prediction error through backpropagation through time (BPTT). By considering \mathbf{a} , the computations of posterior are

$$q(\mathbf{z}_t^{q,a,l} | \mathbf{d}_{t-1}^{a,l}, \mathbf{e}_{t:T}^p, \mathbf{e}_{t:T}^v) = \mathcal{N}(\mathbf{z}_t^{q,a,l}; \boldsymbol{\mu}_t^{q,a,l}, \boldsymbol{\sigma}_t^{q,a,l}) \quad (13)$$

$$\boldsymbol{\mu}_t^{q,a,l} = \tanh(\mathbf{W}_{\mu d}^{a,l} \mathbf{d}_{t-1}^{a,l} + \mathbf{a}_{\mu,t}^{a,l} + \mathbf{b}_{\mu}^{a,l}) \quad (14)$$

$$\boldsymbol{\sigma}_t^{q,a,l} = \exp(\mathbf{W}_{\sigma d}^{a,l} \mathbf{d}_{t-1}^{a,l} + \mathbf{a}_{\sigma,t}^{a,l} + \mathbf{b}_{\sigma}^{a,l}) \quad (15)$$

$$\mathbf{z}_t^{q,a,l} = \boldsymbol{\mu}_t^{q,a,l} + \boldsymbol{\sigma}_t^{q,a,l} * \boldsymbol{\epsilon} \quad (16)$$

where $\boldsymbol{\mu}_t^{q,a,l}$ and $\boldsymbol{\sigma}_t^{q,a,l}$ are mean and variance for the posterior distribution of $\mathbf{z}_t^{q,a,l}$ at time-step t in l th layer in the associative module. Note that the weight matrices for \mathbf{d} are different from those used to compute the prior.

2.4 The proprioception module

Proprioceptive patterns are directly generated from the PV-RNN. The highest layer in the proprioception module receives the input from the lowest layer in the associative layer, and its computations are

$$\mathbf{u}_t^{p,l} = \begin{cases} \mathbf{W}_{dd}^{p,a} \mathbf{d}_t^{a,1} + \mathbf{W}_{dd}^{p,ll} \mathbf{d}_{t-1}^{p,l} + \mathbf{W}_{dz}^{p,l} \mathbf{z}_t^{p,l} + \mathbf{b}^{p,l} & \text{if top layer} \\ \mathbf{W}_{dd}^{p,ll} \mathbf{d}_{t-1}^{p,l} + \mathbf{W}_{dz}^{p,l} \mathbf{z}_t^{p,l} + \mathbf{b}^{p,l} & \text{otherwise} \end{cases} \quad (17)$$

$$\mathbf{h}_t^{p,l} = \left(1 - \frac{1}{\tau^{p,l}}\right) \mathbf{h}_{t-1}^{p,l} + \frac{1}{\tau^{p,l}} \mathbf{u}_t^{p,l} \quad (19)$$

$$\mathbf{d}_t^{p,l} = \tanh(\mathbf{h}_t^{p,l}) \quad (20)$$

Proprioceptive patters are generated from the lowest layer of the proprioception module.

$$\mathbf{p}_t = \tanh(\mathbf{W}^p \mathbf{d}_t^{p,1} + \mathbf{b}^p) \quad (21)$$

2.5 The vision module

For the vision module, a special adjustment was made. Although introducing recurrent connections in convolutional neural networks (CNN) offers great performance (Xingjian et al., 2015) for modelling dynamic visual patterns, it is computationally expensive. Our model is developed to work in physical robots in real time in the future. Therefore, an architecture that is computationally less intensive was needed. In this vision module, PV-RNN layers predict latent dynamics of visual patterns, and the predicted latent dynamics are fed to decoders comprised of static CNNs to generate images. Furthermore, during the error-regression scheme described below, visual patterns are perceived as latent dynamics through an encoder. Then, the prediction error is computed as the discrepancy between the predicted latent patterns and the perceived latent patterns, which is computed in a relatively small dimension, reducing the computational burden. Similar to the proprioception module, the highest layer of the vision module receives input from the lowest layer of the associative layer, and its computations are

$$\mathbf{u}_t^{v,l} = \begin{cases} \mathbf{W}_{dd}^{va} \mathbf{d}_t^{a,1} + \mathbf{W}_{dd}^{v,ll} \mathbf{d}_{t-1}^{p,l} + \mathbf{W}_{dz}^{v,l} \mathbf{z}_t^{v,l} + \mathbf{b}^{v,l} & \text{if top layer} \\ \mathbf{W}_{dd}^{v,ll} \mathbf{d}_{t-1}^{v,l} + \mathbf{W}_{zd}^{v,l} \mathbf{z}_t^{v,l} + \mathbf{b}^{v,l} & \text{otherwise} \end{cases} \quad (22)$$

$$\mathbf{h}_t^{v,l} = \left(1 - \frac{1}{\tau^{v,l}}\right) \mathbf{h}_{t-1}^{v,l} + \frac{1}{\tau^{v,l}} \mathbf{u}_t^{v,l} \quad (24)$$

$$\mathbf{d}_t^{v,l} = \tanh(\mathbf{h}_t^{v,l}) \quad (25)$$

Then the lowest layer of the PV-RNNs predicts the latent dynamics \mathbf{l} , and the visual patterns \mathbf{v} are generated through a decoder.

$$\mathbf{l}_t = \tanh(\mathbf{W}^l \mathbf{d}_t^{v,1} + \mathbf{b}^l) \quad (26)$$

$$\mathbf{v}_t = \text{decoder}(\mathbf{l}_t) \quad (27)$$

In error-regression, the targets of latent dynamics $\bar{\mathbf{l}}$ of visual patters $\bar{\mathbf{v}}$ are computed through an encoder.

$$\bar{\mathbf{l}}_t = \text{encoder}(\bar{\mathbf{v}}_t) \quad (28)$$

To improve the generalization capability of the encoder and decoder, *CoordConv* architecture (Liu et al., 2018) was introduced in them.

2.6 Learning process

The visuo-proprioceptive model is trained by maximizing the evidence lower bound. Thus, given T time-step length of proprioceptive patterns $\mathbf{p}_{1:T}$ and visual patterns $\mathbf{v}_{1:T}$, the cost function to be minimized is defined as

$$\begin{aligned} \text{cost} := & \sum_{t=1}^T \left(\frac{1}{R^p} \|\mathbf{p}_t - \bar{\mathbf{p}}_t\|^2 + \frac{1}{R^v} \|\mathbf{v}_t - \bar{\mathbf{v}}_t\|^2 + \sum_{l \in A} w^l \frac{1}{R^l} D_{\text{KL}}[q(\mathbf{z}_t^l | \mathbf{d}_{t-1}^l, e_{t:T}^p, e_{t:T}^v) \| p(\mathbf{z}_t^l | \mathbf{d}_{t-1}^l)] \right. \\ & \left. + \sum_{l \in P} w^l \frac{1}{R^l} D_{\text{KL}}[q(\mathbf{z}_t^l | \mathbf{d}_{t-1}^l, e_{t:T}^p) \| p(\mathbf{z}_t^l | \mathbf{d}_{t-1}^l)] + \sum_{l \in V} w^l \frac{1}{R^l} D_{\text{KL}}[q(\mathbf{z}_t^l | \mathbf{d}_{t-1}^l, e_{t:T}^v) \| p(\mathbf{z}_t^l | \mathbf{d}_{t-1}^l)] \right) \end{aligned} \quad (29)$$

where A, P, and V represent the associative module, the proprioception module, and the vision module. R^p and R^v are the dimensions of proprioceptive patterns and visual patterns to normalize prediction errors, and R^l is the dimension of the distributions of \mathbf{z} to normalize the KL divergence. Since the prior and posterior distributions are assumed to follow a multivariate Gaussian distribution with diagonal covariant matrix, the KL divergence in the cost function is analytically computed. Given two n dimensional multivariate Gaussian distributions $p(\mathbf{z}) = \mathcal{N}(\mathbf{z}; \boldsymbol{\mu}^p, \boldsymbol{\sigma}^p)$ and $q(\mathbf{z}) = \mathcal{N}(\mathbf{z}; \boldsymbol{\mu}^q, \boldsymbol{\sigma}^q)$ where $\boldsymbol{\mu} = (\mu_1, \mu_2, \dots, \mu_n)^T$ and $\boldsymbol{\sigma} = (\sigma_1, \sigma_2, \dots, \sigma_n)^T$,

$$D_{\text{KL}}[q(\mathbf{z}) \| p(\mathbf{z})] = \sum_{i=1}^n \left(\ln \left(\frac{\sigma_i^p}{\sigma_i^q} \right) + \frac{(\mu_i^p - \mu_i^q)^2 + (\sigma_i^q)^2}{2(\sigma_i^p)^2} - \frac{1}{2} \right) \quad (30)$$

The parameters of the model, including $\boldsymbol{\alpha}$, are optimized using BPTT. To perform error-regression, an encoder was also trained separately.

2.7 Testing method

Ahmadi and Tani (2019) proposed a method to test the trained model in a way that is consistent with concepts of predictive coding and active inference. Since a PV-RNN is a generative model. It does not accept any input; thus, it is not straightforward to test with the model with novel patterns. In testing, weights and biases of the networks are fixed, and the only adaptive variable α is updated (Figure 2). The network has a window with a specified time-step that represents the immediate past for perception. Within the window, the posterior is inferred by means of the error-regression. In the error-regression, an optimal posterior is inferred for a given observation by maximizing the evidence lower bound, and the network makes the best prediction for incoming perception. In this process, the adaptive variable α assigned to the time window is updated through BPTT. Optimization is accomplished in an iterative manner, and after a given number of iterations, the window slides one time-step ahead, and the same process occurs during the next time-step. An example of error-regression in real-time applied to a human-robot interactions through proprioception using PV-RNN is found in (Chame and Tani, 2019).

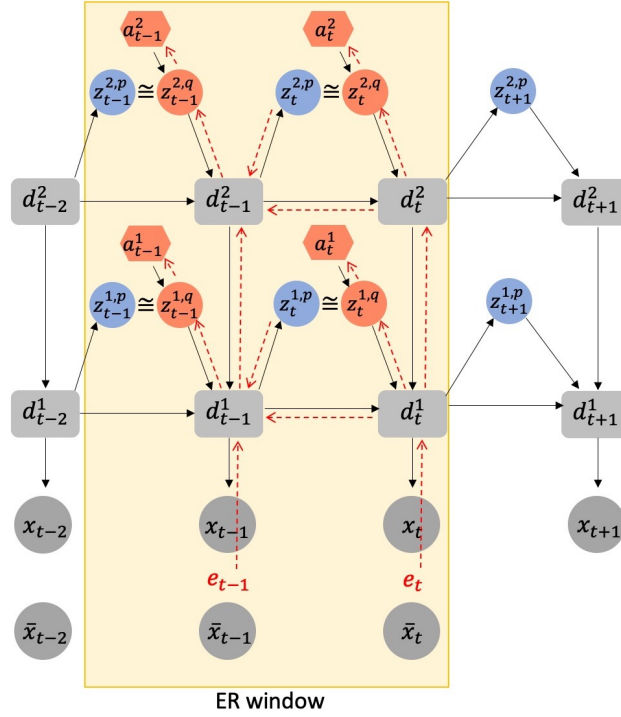


Figure 2: A graphical representation of error-regression. This is an example in which the length of the window is two (the yellow area), and the network has two layers. In error-regression, the weights and the biases of the network are fixed, and only the adaptive variables α are updated. Black arrows represent forward computations, and red arrows indicate how prediction errors are propagated to α by BPTT.

3 Experiments

3.1 Experimental design

Using the proposed model, imitative interaction experiments between a human and a humanoid robot were conducted. Although human-robot interaction ought to be studied in an online fashion to reflect human behavior in response to robot actions, because of the intensive computation required in the error regression scheme, we could not conduct such experiments online. Therefore, the current study examined only the dynamic response of the model network using recorded sequences of visuo-proprioceptive patterns. For this purpose, the dataset containing human-demonstrated movement patterns in terms of visuo-proprioceptive sequences were collected both for training the network and for later testing of pseudo-synchronized imitative interaction. After training, the model was tested with novel visuo-proprioceptive patterns in error-regression with two different scenarios (Experiment 1 and Experiment 2). In Experiment 1, different values of the meta-prior were assigned to the proprioception module and the vision module to examine how regulating complexity in each modality affects coordination of different modalities. In Experiment 2, a set of meta-prior

values in the whole network was shifted to larger or smaller values than those used in the learning phase, in order to examine the effect of regulating complexity on the manner of synchronized imitation. This experimental setting is different from (Chame and Tani, 2019), in which dynamic characteristics during imitative interaction were compared between different networks trained with different values of the meta-prior.

In the following experiments, some parameters that determine the network structure were set as follows. The associative module consisted of a one-layer PV-RNN, and the proprioception module and the vision module consisted of two-layers of PV-RNN, respectively. These PV-RNN layers were characterized by a time scale imposed on MTRNN computation. That is, the higher layer had a larger time constant, producing slow time-scale dynamics, and lower layer had smaller time constants, generating fast time-scale dynamics. Therefore, in this study, the higher layer of the proprioception module and the vision module, which receive input from the associative module, are referred to as the *slow layer*, and the lower layer is referred to as the *fast layer*.

3.2 Data preparation

To obtain a dataset of synchronized vision and proprioception, we used a humanoid robot, Torobo (Tokyo Robotics Inc.) and a motion capture suit (Perception Neuron, Noitom Ltd.). Torobo is a human-sized, torso-type humanoid robot with 16 joint-angles, of which 6 are for each arm and 4 are for the torso and head positions. Human body movements can be mapped to joint-angle trajectories of the robot using the motion capture suit. A human experimenter wearing the suit demonstrated a set of body movements, which were mapped as joint-angle trajectories. This demonstration was also recorded with a camera to obtain corresponding visual patterns. The target sequential movement pattern to be learned by the robot was designed by considering a probabilistic finite state machine that can generate probabilistic sequences of three different primitive movement patterns. Those were (A) waving with both arms three times, (B) rotating the torso to the left with the arms, and (C) rotating the torso to the right with the arms. Primitive pattern A is followed either by primitive pattern B or primitive pattern C with a 50% chance, and primitive patterns B and C are followed by pattern A with 100% chance (Figure 3 (A)). One sequence consists of 8 probabilistic transitions of primitive movements, and movement sequences demonstrated by three human participants were recorded for 10 sequences for each. In other words, the dataset was comprised of 30 sequences of visuo-proprioceptive temporal patterns. Recorded visuo-proprioceptive patterns were down-sampled to 3.75 Hz so that one sequence became 400 time-steps. Joint-angle trajectories were normalized to a range between -1 and 1 . Vision patterns were further converted into gray scale images and down-sized to 64×64 pixels (Figure 3 (B)). It is noted that the visual trajectories are far more fluctuated than the proprioceptive ones due to various optical conditions, such as illumination and surface reflectiveness.

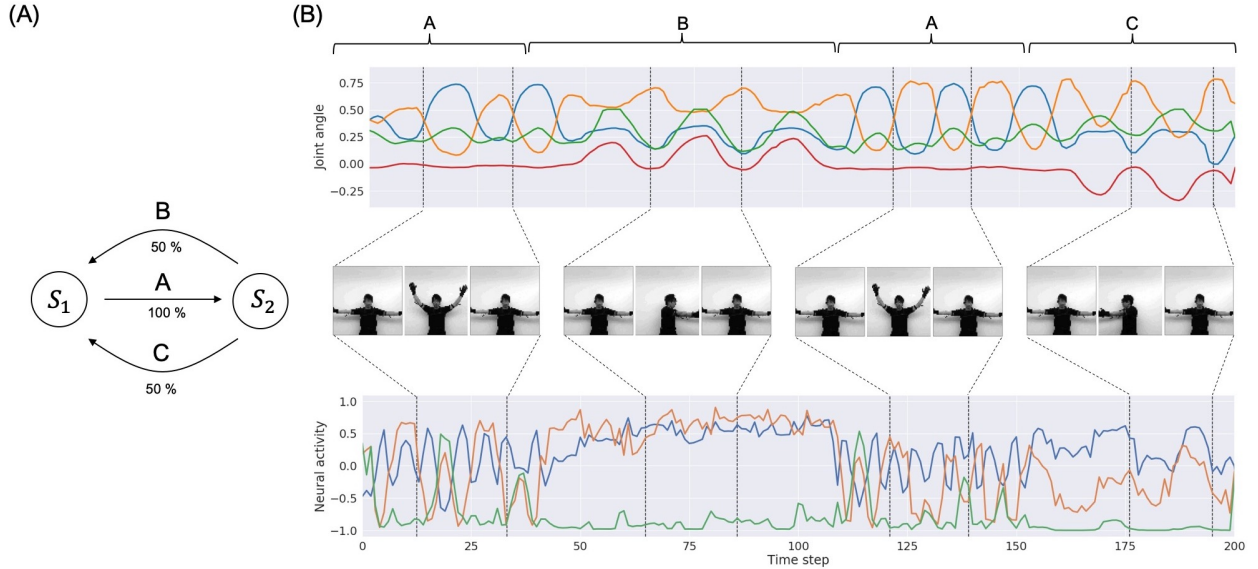


Figure 3: Training data. (A) A diagram of the probabilistic finite state machine. (B) An example of the training dataset. The top row is a part of a joint-angle trajectory. The corresponding labels of primitive patterns are (A, B, and C) indicated above the plots. For simplicity, only 4 joint-angles out of 16 representing the movements are shown. The middle row show the corresponding visual pixel images at each period. The bottom row shows visual trajectories in the latent space embedded by the encoder. For simplicity, only three variables out of 20 are shown.

By using the training example, the model is required to extract a probabilistic structure that the primitive pattern of B or C appears with only a 50% chance after every appearance of the primitive A by estimating precision in transitions of primitives by learning. Such learning should be achieved without providing explicit labels for those primitives, but by extracting the underlying chunking and segmentation structure from the continuous sensory signals prepared in the dataset. The PV-RNN can achieve such tasks by using the multiple timescale RNN scheme combined with Bayesian inference approach (Ahmadi and Tani, 2019).

3.3 Experiment 1: Different meta-priors in different modalities

In this experiment, we examined how assigning different meta-priors to the proprioception and vision modules affects the learning process and error-regression performance. Two sets of meta-priors w_1 and w_2 were assigned to the model (Table 1). w_1 has larger values of the meta-prior in the proprioception module than in the vision module, and they were exchanged in w_2 . Both w_1 and w_2 have the same value for the meta-prior in the associative module. First, the model was trained with the w_1 and w_2 , and the learning process was examined, with special attention to each component of the lower bound. To facilitate training, Adam optimizer (Kingma and Ba, 2014) was utilized with the parameter setting $\alpha = 0.001$, $\beta_1 = 0.9$, and $\beta_2 = 0.999$. The model was trained 10 times with different random initializations of the parameters of the model for 10,000 epochs, and the mean and standard deviation of the prediction error of proprioception and vision, and the KL divergence of each layer of the model at each epoch were computed. Results are

	\mathbb{R}^d	\mathbb{R}^z	τ	w_1	w_2
Associative module	10	1	15	0.0025	0.0025
Proprioception slow layer	20	2	8	0.005	0.0025
Proprioception fast layer	30	3	2	0.01	0.005
Vision slow layer	20	2	8	0.0025	0.005
Vision fast layer	30	3	2	0.005	0.01

Table 1: The model configuration in Experiment 1. \mathbb{R}^d and \mathbb{R}^z are the dimensions of d and z , respectively. τ is the time constant of MTRNN computation in each layer.

summarized in Figure 4. In comparing w_1 and w_2 conditions, even though the prediction errors in the proprioception and vision modules showed similar behavior (Figure 4 (A), (B)), the KL divergence in each module was optimized differently. Despite different values of the meta-prior assigned to the fast layer of the proprioception module, its KL divergences in w_1 and w_2 conditions were reduced in exactly the same way (Figure 4 (E)). This is not the case in the fast layer of the vision module (Figure 4 (G)). The KL divergence in the slow layer of the proprioception module and the slow layer of the vision module showed different values in w_1 and w_2 settings (Figure 4 (D),(F)). Interestingly, although the associative module was set to the same value of meta-prior in w_1 and w_2 conditions, the KL divergence in the w_2 setting reached a larger value than that in the w_1 setting. This is because the larger value of the meta-prior assigned to the fast layer of the vision module in the w_2 condition prevented the vision module from absorbing the fluctuation in the observed visual patterns, which resulted in bottom-up fluctuation from the vision module to the associative module, appearing as a discrepancy between the prior and the posterior in this module. Because visual sensation tends to contain more inherent randomness compared to proprioceptive sensation as described previously, complexity in this modality should be adequately regulated by setting a smaller meta-prior value. Otherwise, the discrepancy that appears in the visual module tends to leap to the higher associative module without being well resolved before.

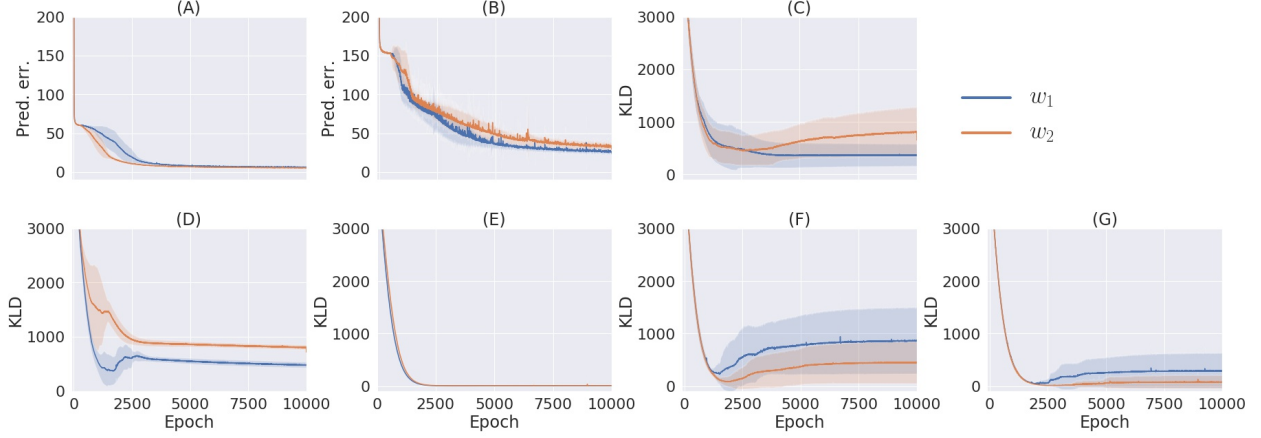


Figure 4: The learning process of the model with two different meta-prior settings. (A) The prediction error in proprioception. (B) The prediction error in vision. (C) The KL divergence in the associative module. (D) The KL divergence in the slow layer of the proprioception module. (E) The KL divergence in the fast layer of the proprioception module. (F) The KL divergence in the slow layer of the vision module. (G) The KL divergence in the fast layer of the vision module. The shadows are the standard deviation of 10 trials with different parameter initializations. Note that the values of prediction errors are the sum of the prediction errors at all time-steps and sequences normalized by the dimension of data.

We further tested the trained models in the error-regression scheme. Training of the models stopped after 4,000 epochs. Novel visuo-proprioceptive patterns were prepared for the error-regression, which also comprised the previous primitive body movements A, B, and C, the lengths of which were 400 time-steps. The length of the time window was set at 30, and the number of iterations of optimization by BPTT at each time-step was 30. As in learning, Adam was used to improve optimization with the parameter settings $\alpha = 0.2$, $\beta_1 = 0.9$, and $\beta_2 = 0.999$. Evaluation of the error-regression examined how much the reconstruction error in each modality and the KL divergence at each subnetwork in the PV-RNN were minimized. That is, at the point when T' time-step window length for the immediate past shifts t times, the adaptive variable \mathbf{a} assigned within the window is optimized with the iterative process, and at the last iteration, the reconstruction error and the KL divergence are computed inside the window. Therefore, they are defined as

$$\text{Proprioception error} := \frac{1}{T} \sum_{t=1}^T \frac{1}{T'} \sum_{t'=1}^{T'} \frac{1}{R^p} \|\mathbf{p}_{t'} - \bar{\mathbf{p}}_{t'}\|^2 \quad (31)$$

$$\text{Vision error} := \frac{1}{T} \sum_{t=1}^T \frac{1}{T'} \sum_{t'=1}^{T'} \frac{1}{R^l} \|\mathbf{l}_{t'} - \bar{\mathbf{l}}_{t'}\|^2 \quad (32)$$

$$\text{KLD} := \frac{1}{T} \sum_{t=1}^T \frac{1}{T'} \sum_{t'=1}^{T'} \frac{1}{R^z} D_{\text{KL}}[q(\mathbf{z}_{t'} | \mathbf{d}_{t'-1}, e_{t':T}) \| p(\mathbf{z}_{t'} | \mathbf{d}_{t'-1})] \quad (33)$$

where t' is the time step inside the window. R^p and R^l are the dimension of proprioception and the latent space of vision, respectively. R^z is the dimension of \mathbf{z} , and the KL divergence is computed for every PV-RNN submodule. Models trained in previous experiments were used. Error-regression was run 10 times with different random number seeds, and the mean and standard deviation of each quantity were computed. In addition, one-step look-ahead prediction error, the discrepancy between the prediction in the next time-step of the current window and the observation, was computed in vision to evaluate the prediction accuracy.

Results are summarized in Table 2. The prediction error in proprioception was remarkably minimized compared to that in vision, in both conditions w_1 and w_2 . This is because the visual modality contains more noise than the proprioceptive modality. It was also observed that the reconstruction error in vision was smaller for the w_1 condition than the w_2 condition. Furthermore, the KL divergence in the associative module was reduced more significantly in the w_1 condition than the w_2 condition. This resulted because the vision module generalized better with noisy visual patterns in the test of error regression in the w_1 case than the w_2 case by minimizing the complexity term more. Because fluctuation or randomness in visual sensation was well resolved within the vision module in the w_1 case, the associative module became relatively free from such fluctuation, as evidenced by the smaller KL divergence observed in the associative

module under this condition of minimizing the complexity term. As a result, the one-step, look-ahead prediction was also more accurate in w_1 condition.

	Proprioception reconstruction error	Vision reconstruction error	Associative KLD	Proprioception slow KLD
w_1	$0.017 \pm 9.5 \times 10^{-4}$	$0.12 \pm 6.9 \times 10^{-3}$	2.0 ± 0.091	1.6 ± 0.12
w_2	$0.011 \pm 2.9 \times 10^{-4}$	$0.19 \pm 1.5 \times 10^{-2}$	3.2 ± 0.15	2.6 ± 0.11
	Proprioception fast KLD	Vision slow KLD	Vision fast KLD	Vision one-step prediction error
w_1	0.57 ± 0.040	8.1 ± 0.17	0.50 ± 0.048	0.20 ± 0.0097
w_2	0.57 ± 0.041	1.9 ± 0.071	0.54 ± 0.048	0.24 ± 0.017

Table 2: The result of error regression. The errors are the standard deviation of 10 different trials with different random number seeds.

3.4 Experiment 2: Different meta-priors of the whole system

Based on Experiment 1, we further investigated how values of the meta-prior of the whole system affect interactions with a human. The model that was trained for 4,000 epochs in Experiment 1 with the w_1 setting was used. Five different meta-prior settings were prepared: from smaller values of the meta-prior setting W_1 to the larger setting W_5 with a consistent ratio among layers (Table 3). Error-regression with different meta-prior settings was performed with the novel visuo-proprioceptive patterns used in Experiment 1. As in the previous experiment, the error-regression was run 10 times with different random number seeds, and the mean and variance of each quantity introduced in the previous experiment were computed. In this experiment, one-step look-ahead prediction error in proprioception was also measured.

	W_1	W_2	W_3	W_4	W_5
Associative module	2.5×10^{-5}	2.5×10^{-4}	2.5×10^{-3}	2.5×10^{-2}	2.5×10^{-1}
Proprioception slow layer	5.0×10^{-5}	5.0×10^{-4}	5.0×10^{-3}	5.0×10^{-2}	5.0×10^{-1}
Proprioception fast layer	1.0×10^{-4}	1.0×10^{-3}	1.0×10^{-2}	1.0×10^{-1}	1.0
Vision slow layer	2.5×10^{-5}	2.5×10^{-4}	2.5×10^{-3}	2.5×10^{-2}	2.5×10^{-1}
Vision fast layer	5.0×10^{-5}	5.0×10^{-4}	5.0×10^{-3}	5.0×10^{-2}	5.0×10^{-1}

Table 3: The values of meta-prior in Experiment 2.

The results are summarized in Figure 5. As a whole, with smaller values of the meta-prior, the reconstruction error was minimized more (Figure 5(A)), and the KL divergence remained large (Figure 5(D)), whereas with larger values of the meta-prior, the KL divergence was minimized more (Figure 5(D)), and the reconstruction error remained large (Figure 5(A)). This tendency can also be seen in the local proprioception module and vision module. In the proprioception module, as the values of meta-prior increased, the reconstruction error in proprioception became large (Figure 5(B)), and the KL divergence became small, both in the slow layer (Figure 5(F)) and in the fast layer (Figure 5(G)). Similarly, in the vision module, as the values of meta-prior increased, the reconstruction error in vision increased (Figure 5(C)), and the KL divergence became small both in the slow layer (Figure 5(H)) and in the fast layer (Figure 5(I)). The KL divergence at the associative module also increased as the values of the meta-prior increased (Figure 5(E)). In addition, with smaller values of the meta-prior, the one-step, look-ahead prediction error was minimized more both in proprioception (Figure 5(J)) and in vision (Figure 5(K)).

This is because the KL divergence term in the evidence lower bound was weighted more for minimization than was the reconstruction error term. In this situation, the posterior $q(z_t | \mathbf{d}_{t-1}, e_{t:T'})$ at each time step in the error regression window (ER-W) approached its prior $p(z_t | \mathbf{d}_{t-1})$ in the window by modulating the adaptive value \mathbf{a}_t , which is fed into the computation of the posterior $q(z_t | \mathbf{d}_{t-1}, e_{t:T'})$, while the prior $p(z_t | \mathbf{d}_{t-1})$ was less changed. This means that network dynamics were driven mainly by the prior, while less affected by sensory inputs. Network dynamics become more egocentric by following the prior, which was less modified by weaker regulation of the complexity term (i.e., more weighting for the KL divergence term). On the other hand, with more weighting (i.e., less weighting for the KL divergence term), network dynamics became more adaptive to change or fluctuations of sensory inputs, by freely

modulating the posterior in the direction of error minimization without being much constrained by the prior. In this condition, the prior $p(z_t|\mathbf{d}_{t-1})$ at each step in the window also changes because the posterior $q(z_{t-1}|\mathbf{d}_{t-2})$ at the previous step, which is mapped to $p(z_t|\mathbf{d}_{t-1})$ through \mathbf{d}_t also changes.

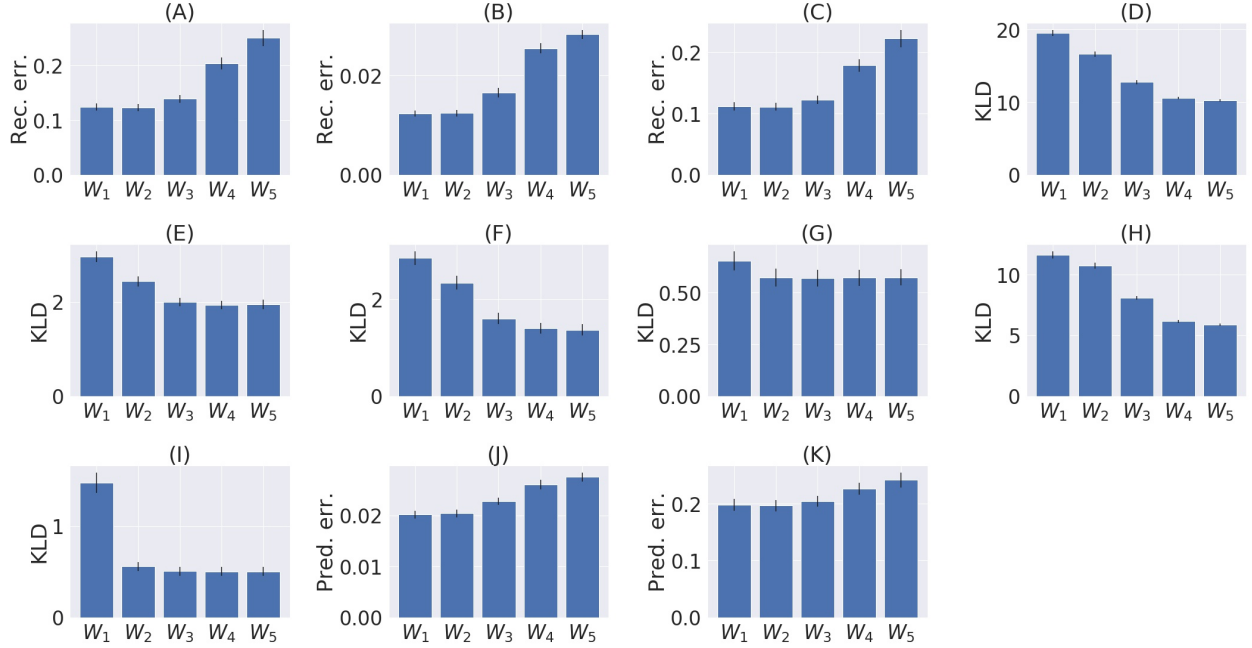


Figure 5: Reconstruction error, KL divergence minimization, and one-step, look-ahead prediction error in error-regression with five meta-prior settings. (A) Sum of the reconstruction error in proprioception and vision. (B) The reconstruction error in proprioception. (C) The reconstruction error in vision. (D) Sum of the KL divergence at all layers. (E) The KL divergence in the associative module. (F) The KL divergence in the slow layer of the proprioception module. (G) The KL divergence in the fast layer of the proprioception module. (H) The KL divergence in the slow layer of the vision module. (I) The KL divergence of the fast layer of the vision module. (J) One-step, look-ahead prediction error in proprioception. (K) One-step, look-ahead prediction error in vision. Error bars represent the standard deviation of 10 trials with different random seeds. Note that each graph has a different scale.

Figure 6 (A) and (B) shows an example of time-series plots of related neural activities of the proprioception module, comparing these two cases of strong (W_1 setting) and weak (W_5 setting) regulation of the complexity term. Both cases are computed for a situation observing the same visuo-proprioceptive sequence pattern. With strong regulation of the complexity term (Figure 6 (A) top), the observation (dashed lines) was well-reconstructed in the reconstructed outputs (real lines) inside the ER-W (shaded area) from time-step 120 to 150 due to relatively stronger weighting in the accuracy term compared to W_5 setting. The plots after time-step 150 represent future prediction of expecting to encounter the primitive B. From time-steps 150 to 180 (Figure 6 (A) bottom), the robot observed new sensory information where the primitive C instead of the predicted primitive of B was encountered. (Remember that there is a 50% chance of encountering the primitive B or the primitive C.) This new observation was reconstructed inside the ER-W, and based on the inferred posterior during this period, the robot updated the future prediction after time-step 180 as the primitive C to be continued. Because of relatively stronger weighting in the accuracy term, the posterior was inferred to adapt to reality. The prediction was also updated accordingly (Figure 6 (A) bottom).

In the case of weak regulation (Figure 6(B)top), the observation was still well reconstructed inside the ER-W. This is because primitive A always follows primitives either B or C so that it is easy to predict primitive A. Therefore, the reconstruction error inside the ER-W was small from the beginning. The plots after time-step 150 represent future predictions of expecting primitive B to be encountered. After observing new sensory information in which primitive C instead of the predicted primitive C was encountered between time-step 150 and 180 (Figure 6(B)bottom), however, the new observation was not reconstructed well inside the ER-W. Due to strong regulation of the KL divergence term (weak regulation of the complexity term), the posterior was forced closer to the prior by ignoring the new observation. Consequently, the inferred posterior did not affect the prior as much as in the W_1 setting, which resulted in generation of consistent prediction for future. Actually, the look-ahead prediction made at time-step 150, shown in the top row, and the one made at time-step 180 in the bottom row are almost the same. These observations imply that both the prediction of the future and the reflection of the past become more adaptive to sensory observation in the case of

stronger regulation of the complexity term, whereas they become more persistent regardless of the sensory observation in the case of weaker regulation.

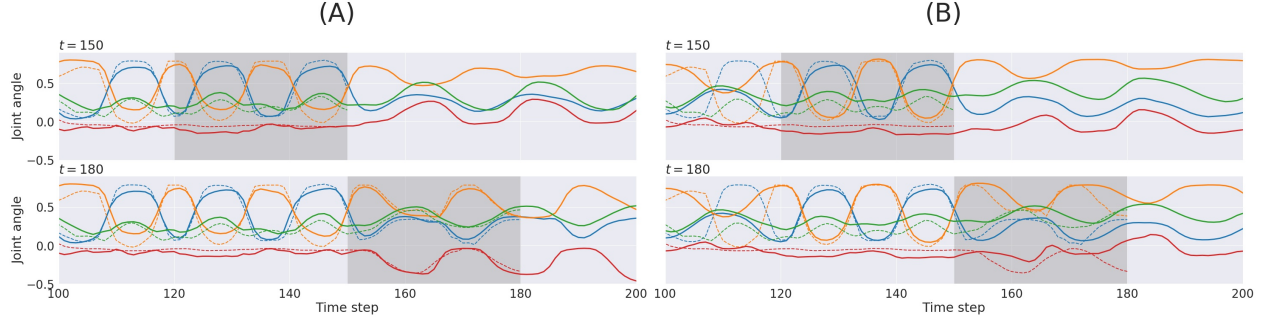


Figure 6: An example of time-series plots of neural activities in the output layer of proprioception module in W_1 setting (A) and in W_5 setting (B). The reconstruction of the past observation and the future prediction at time-step 150 (top) and at time-step 180 (bottom) are shown. The solid lines represent the neural activities, and the dashed lines represent the observations. The shadow area indicates the error-regression window. For simplicity, only 4 out of 16 joint-angles representing the movements are shown.

Some representative videos related to Experiment 2 can be seen in video link A and in video link B for W_1 condition and W_5 condition, respectively. These videos show how prediction of future as well as reflection of past can be performed for each condition. Also, further temporal details during the error regression process can be seen in video link C and in video link D for W_1 condition and W_5 condition, respectively. In these videos, it can be observed that there are some divergence between the prior and the posterior in terms of mean and variance and that they are dynamically changing inside the ER-W in W_1 condition whereas these two profiles become close each other with showing relatively persistent patterns in W_5 condition. These observations accord with our analysis described previously.

4 Discussion

In this study, we hypothesized that the means of regulating the complexity term in the evidence lower bound in the model contributes greatly to two distinct properties of agents: coordination of multimodal perception and strength of intention or belief in acting with others. We evaluated the hypotheses by building a model for multimodal imitative interaction of agents using visuo-proprioceptive sensory modalities, based on frameworks of predictive coding and active inference, and by conducting experiments on imitative human-robot interactions.

We performed experiments in two different scenarios. First, the ratio of regulating the complexity term was changed between the vision module and the proprioception module. Our results show that the complexity term in the vision module should be regulated more than that of the proprioception module. This is because visual sensory and proprioceptive inputs are fundamentally different with respect to their intrinsic randomness. Visual inputs fluctuate more often due to various optical conditions, such as illumination and surface reflectiveness. In this situation, the complexity of information processing in the vision module should be more regulated to achieve better generalization.

Second, regulation strength for the complexity term throughout the whole network was varied after learning. Our results demonstrated that this significantly affects the manner of generating human-robot interaction. With weaker regulation of the complexity term, the robot tends to act more egocentrically, without adapting to the other. In contrast, with stronger regulation of the complexity term, the robot tends to follow its human counterpart by adapting its internal state. This result implies that the strength of intention or belief in acting with others can be modulated by adjusting the strength of regulation of the complexity term after the learning phase.

In the current study, we evaluated the hypotheses using imitative human-robot interactions. In imitative interactions between a human and a robot, there are two scenarios: the robot following the human’s movements, and the human following the robot’s movements. In our experimental setup, the agent with strong regulation of the complexity term corresponds to the former case, and that with weak regulation to the latter. This may provide new insights into studies of mirror neuron systems (Rizzolatti and Fogassi, 2014; Kilner et al., 2007). Mirror neurons were first discovered in area F5 of the monkey premotor cortex (Di Pellegrino et al., 1992; Gallese et al., 1996), and it was reported that mirror neurons are activated while executing their own actions, as well as observing those performed by others. Because mirror neurons transfer observations of an action to generation of the same action, they could underlie the mechanism of imitative behaviors, which are thought to be the basis of various higher cognitive functions (Aly and Tapus, 2015;

Kohler et al., 2002; Oztup et al., 2006, 2013). These considerations imply that imitation by mirror neurons can be explained by the current model in the case of strong regulation of the complexity term.

However, in everyday social interactions, humans do not just follow others, but they also lead them with their own belief, depending on each contextual or social situation. Psychological studies indicate that turn-taking between following and leading can take place rather spontaneously in various social cognitive behaviors, including conversation (Sacks et al., 1978), mother-infant pre-verbal communication (Trevvarthen, 1979) and imitation (Nadel, 2002). In considering possible underlying mechanisms for turn-taking, some researchers (Ikegami and Iizuka, 2007; Ito and Tani, 2004) suggest that turn-taking may develop due to potential instability, such as chaos formed in coupled dynamics between two agents in their modeling studies. We could consider a meta-level dynamic of coupling two agents, whereby the value of the meta-prior for regulating the complexity term for each agent counteracts mutually. This could result in autonomous shifts between the leading mode by increasing the meta-prior and the following mode by reducing it.

Future studies should examine the aforementioned mechanism for turn-taking by conducting an online experiment of human-robot interactions. However, the computational cost of online error regression for inference of the posterior has been the major bottleneck for conducting such experiments in real time and this is why the current study was limited to using recorded visuo-proprioceptive sequence patterns as the target in testing synchronized imitation, rather than introducing actual, real-time, human-robot interaction. Regarding this problem, some may suggest employing other types of variational models, such as a variational recurrent neural network (VRNN) (Chung et al., 2015), because a VRNN demands far less computation time, since the posterior at each time step can be inferred by simple sequential mapping of inputs using an autoencoder (Kingma et al., 2016). However, it is argued that the current scheme for inference of the posterior through iterative computation for optimization should be vital for any embodied cognitive systems that require rapid adaptation of the internal states to the environment. Actually, Ahmadi and Tani (Ahmadi and Tani, 2019) showed that PV-RNN can perform better than VRNN (Chung et al., 2015) in an online prediction in dynamically changing environment by inferring the posterior using the error regression scheme. Therefore, future studies are expected to explore possible methods for accelerating online error regression of the model, such as by massive parallelisation for the purpose of conducting real-time, human-robot interactions using the model.

Acknowledgments

This work was supported by funding from Okinawa Institute of Science and Technology Graduate University. We thank the lab members in the Cognitive Neurorobotics Research Unit. Especially, we are grateful to Ahmadreza Ahmadi and Prasanna Vijayaraghavan for their help in developing the model. We thank Siqing Hou for his help in collecting the dataset. We also thank Dr. Steven Aird for assisting improving the manuscript.

References

- Ahmadi, A. and Tani, J. (2019). A novel predictive-coding-inspired variational rnn model for online prediction and recognition. *Neural computation* 31, 2025–2074
- Aly, A. and Tapus, A. (2015). An online fuzzy-based approach for human emotions detection: An overview on the human cognitive model of understanding and generating multimodal actions. In *Intelligent assistive robots* (Springer). 185–212
- Baltieri, M. and Buckley, C. L. (2017). An active inference implementation of phototaxis. In *Artificial Life Conference Proceedings 14* (MIT Press), 36–43
- Buckley, C. L., Kim, C. S., McGregor, S., and Seth, A. K. (2017). The free energy principle for action and perception: A mathematical review. *Journal of Mathematical Psychology* 81, 55–79
- Chame, H. F. and Tani, J. (2019). Cognitive and motor compliance in intentional human-robot interaction. *arXiv preprint arXiv:1911.01753* Accepted for publication in IEEE ICRA2020
- Choi, M. and Tani, J. (2018). Predictive coding for dynamic visual processing: Development of functional hierarchy in a multiple spatiotemporal scales rnn model. *Neural computation* 30, 237–270
- Chung, J., Kastner, K., Dinh, L., Goel, K., Courville, A. C., and Bengio, Y. (2015). A recurrent latent variable model for sequential data. In *Advances in neural information processing systems*. 2980–2988
- Clark, A. (2015). *Surfing uncertainty: Prediction, action, and the embodied mind* (Oxford University Press)
- Di Pellegrino, G., Fadiga, L., Fogassi, L., Gallese, V., and Rizzolatti, G. (1992). Understanding motor events: a neurophysiological study. *Experimental brain research* 91, 176–180
- Friston, K. (2005). A theory of cortical responses. *Philosophical transactions of the Royal Society B: Biological sciences* 360, 815–836

- Friston, K. (2018). Does predictive coding have a future? *Nature neuroscience* 21, 1019
- Friston, K., Mattout, J., and Kilner, J. (2011). Action understanding and active inference. *Biological cybernetics* 104, 137–160
- Friston, K. J., Daunizeau, J., and Kiebel, S. J. (2009). Reinforcement learning or active inference? *PloS one* 4, e6421
- Friston, K. J., Daunizeau, J., Kilner, J., and Kiebel, S. J. (2010). Action and behavior: a free-energy formulation. *Biological cybernetics* 102, 227–260
- Gallese, V., Fadiga, L., Fogassi, L., and Rizzolatti, G. (1996). Action recognition in the premotor cortex. *Brain* 119, 593–609
- Hohwy, J. (2013). *The predictive mind* (Oxford University Press)
- Huys, R., Daffertshofer, A., and Beek, P. J. (2004). Multiple time scales and multi-form dynamics in learning to juggle. *Motor control* 8, 188–212
- Hwang, J., Kim, J., Ahmadi, A., Choi, M., and Tani, J. (2018). Dealing with large-scale spatio-temporal patterns in imitative interaction between a robot and a human by using the predictive coding framework. *IEEE Transactions on Systems, Man, and Cybernetics: Systems*
- Ikegami, T. and Iizuka, H. (2007). Turn-taking interaction as a cooperative and co-creative process. *Infant Behavior and Development* 30, 278–288
- Ito, M. and Tani, J. (2004). On-line imitative interaction with a humanoid robot using a dynamic neural network model of a mirror system. *Adaptive Behavior* 12, 93–115
- Kawato, M., Furukawa, K., and Suzuki, R. (1987). A hierarchical neural-network model for control and learning of voluntary movement. *Biological cybernetics* 57, 169–185
- Kilner, J. M., Friston, K. J., and Frith, C. D. (2007). Predictive coding: an account of the mirror neuron system. *Cognitive processing* 8, 159–166
- Kingma, D. P. and Ba, J. (2014). Adam: A method for stochastic optimization. *arXiv preprint arXiv:1412.6980*
- Kingma, D. P., Salimans, T., Jozefowicz, R., Chen, X., Sutskever, I., and Welling, M. (2016). Improved variational inference with inverse autoregressive flow. In *Advances in neural information processing systems*. 4743–4751
- Kohler, E., Keysers, C., Umiltà, M. A., Fogassi, L., Gallese, V., and Rizzolatti, G. (2002). Hearing sounds, understanding actions: action representation in mirror neurons. *Science* 297, 846–848
- Kording, K. P., Tenenbaum, J. B., and Shadmehr, R. (2007). The dynamics of memory as a consequence of optimal adaptation to a changing body. *Nature neuroscience* 10, 779–786
- LeCun, Y., Boser, B., Denker, J. S., Henderson, D., Howard, R. E., Hubbard, W., et al. (1989). Backpropagation applied to handwritten zip code recognition. *Neural computation* 1, 541–551
- LeCun, Y., Bottou, L., Bengio, Y., and Haffner, P. (1998). Gradient-based learning applied to document recognition. *Proceedings of the IEEE* 86, 2278–2324
- Lee, T. S. and Mumford, D. (2003). Hierarchical bayesian inference in the visual cortex. *JOSA A* 20, 1434–1448
- Liu, R., Lehman, J., Molino, P., Such, F. P., Frank, E., Sergeev, A., et al. (2018). An intriguing failing of convolutional neural networks and the coordconv solution. In *Advances in Neural Information Processing Systems*. 9605–9616
- Nadel, J. (2002). Imitation and imitation recognition: Functional use in preverbal infants and nonverbal children with autism. *The imitative mind: Development, evolution, and brain bases* 4262
- Newell, K. M., Liu, Y.-T., and Mayer-Kress, G. (2001). Time scales in motor learning and development. *Psychological review* 108, 57
- Oliver, G., Lanillos, P., and Cheng, G. (2019). Active inference body perception and action for humanoid robots. *arXiv preprint arXiv:1906.03022*
- Oztop, E., Kawato, M., and Arbib, M. (2006). Mirror neurons and imitation: A computationally guided review. *Neural networks* 19, 254–271
- Oztop, E., Kawato, M., and Arbib, M. A. (2013). Mirror neurons: functions, mechanisms and models. *Neuroscience letters* 540, 43–55
- Pezzulo, G., Rigoli, F., and Friston, K. J. (2018). Hierarchical active inference: A theory of motivated control. *Trends in cognitive sciences* 22, 294–306
- Rao, R. P. and Ballard, D. H. (1999). Predictive coding in the visual cortex: a functional interpretation of some extra-classical receptive-field effects. *Nature neuroscience* 2, 79

- Rizzolatti, G. and Fogassi, L. (2014). The mirror mechanism: recent findings and perspectives. *Philosophical Transactions of the Royal Society B: Biological Sciences* 369, 20130420
- Rumelhart, D. E., Hinton, G. E., and Williams, R. J. (1985). *Learning internal representations by error propagation*. Tech. rep., California Univ San Diego La Jolla Inst for Cognitive Science
- Sacks, H., Schegloff, E. A., and Jefferson, G. (1978). A simplest systematics for the organization of turn taking for conversation. In *Studies in the organization of conversational interaction* (Elsevier). 7–55
- Smith, M. A., Ghazizadeh, A., and Shadmehr, R. (2006). Interacting adaptive processes with different timescales underlie short-term motor learning. *PLoS biology* 4
- Tani, J. and Nolfi, S. (1999). Learning to perceive the world as articulated: an approach for hierarchical learning in sensory-motor systems. *Neural Networks* 12, 1131–1141
- Trevarthen, C. (1979). Communication and cooperation in early infancy: A description of primary intersubjectivity. *Before speech: The beginning of interpersonal communication* 1, 530–571
- Werbos, P. (1974). Beyond regression: New tools for prediction and analysis in the behavioral sciences. *Ph. D. dissertation, Harvard University*
- Xingjian, S., Chen, Z., Wang, H., Yeung, D.-Y., Wong, W.-K., and Woo, W.-c. (2015). Convolutional lstm network: A machine learning approach for precipitation nowcasting. In *Advances in neural information processing systems*. 802–810
- Yamashita, Y. and Tani, J. (2008). Emergence of functional hierarchy in a multiple timescale neural network model: a humanoid robot experiment. *PLoS computational biology* 4, e1000220